Roll-modes generated in turbulent boundary layers with passive surface modifications

Bagus Nugroho,* and Kevin,* and Jason P. Monty,† and Nicholas Hutchins,‡
The University of Melbourne, Parkville ,Victoria, 3010, Australia

Ebenezer P. Gnanamanickam,§
Embry-Riddle Aeronautical University, Daytona Beach ,Florida, 32114, USA

A unique class of directional surfaces arranged in a converging-diverging (herringbone) pattern are studied experimentally in a zero pressure gradient turbulent boundary layers. Hot-wire measurements using both single and cross-wire show that these small surfaces are able to generate large-scale counter rotating roll-modes/vortices within the turbulent boundary layer, resulting in dramatic spanwise variation in the boundary layer thickness δ (50% variation for the strongest case). The results reveal that above the converging region, the local mean velocity decreases while the turbulence intensity increases, resulting in locally thicker boundary layer. Over the diverging region, the opposite situation occurs, where the mean velocity increases and the turbulence intensity decreases, resulting in a locally thinner boundary layer. The strong perturbation effect from these surfaces to the overall flow dynamics seems unusual, considering that their peak-to-trough height is approximately only 1% of the boundary layer thickness. This study, also investigates the behavior of the large-scale counter-rotating roll-modes when the surface reverts from the herringbone pattern back to the smooth wall, to see how far they persist over the smooth wall. Our preliminary results show that the roll-modes above the smooth wall still persist even at 40δ downstream. The results of this study show that the herringbone surface roughness pattern can act as a novel method of generating counter rotating roll-modes (vortices) for flow control purposes in various engineering applications.

Nomenclature

x	Streamwise direction/distance, m
y	Spanwise direction/distance, m
z	Wall-normal direction/distance, m
U	Mean streamwise velocity, m/s
V	Mean spanwise velocity, m/s
W	Mean wall-normal velocity, m/s
U_∞	Freestream velocity, m/s
U_τ	Skin friction velocity, m/s
U_{sa}	Spanwise averaged mean velocity, m/s
δ	Boundary layer thickness, m
δ_s	Boundary layer thickness over smooth wall, m
δ_r	Boundary layer thickness over rough surface, m
δ_{sa}	Boundary layer thickness averaged over one spanwise wavelength, m
δ_{r_s}	Boundary layer thickness averaged over one spanwise wavelength of rough to smooth case, m

*Graduate Student, Department of Mechanical Engineering
†Senior Lecturer, Department of Mechanical Engineering
‡Associate Professor, Department of Mechanical Engineering
§Assistant Professor, Department of Aerospace Engineering

ν	Kinematic viscosity, m^2/s
Re_τ	Friction Reynolds number
$\overline{u^2}$	Turbulence intensity, m^2/s^2
$\overline{u^2}_{sa}$	Spanwise averaged turbulence intensity, m^2/s^2
α	Riblet yaw angle, $^\circ$
β	Riblet tip angle, $^\circ$
r_s	Separation distance from rough to smooth wall, m
s	Riblet spacing, mm
s^+	Viscous-scaled riblet spacing
h	Riblet height, mm
h^+	Viscous-scaled riblet height
A	Riblet cross-section area, m^2
A^+	Viscous riblet cross-section area
ℓ^+	Square root of viscous riblet cross-section area
Λ	One spanwise length, mm
F_x	Fetch distance, m
l	Hot-wire etched length, mm
l^+	Hot-wire etched viscous-scaled length
d	Hot-wire etched diameter, mm

I. Introduction

Inspired by the microscopic skin topology of fast swimming sharks, flow control in turbulent boundary layers by surface modification (such as riblets) has attracted much attention due to its ability to substantially reduce skin friction drag (Walsh,[1] Choi,[2] Bechert and Bartenwerfer,[3] Bechert et al,[4] Dean and Bushan[5]). The quest for skin friction drag reduction was initially spurred by the 1970's oil crisis, which forced many aerospace and naval industries to minimise their fuel consumption. One of the earliest detailed skin-friction drag reduction studies using riblets was performed by Walsh,[1,6] where linearly arranged small scalloped or triangular riblets (with viscous scale spacing $s^+ = sU_\tau/\nu = 15 - 20$) were able to reduce skin friction drag by up to 8%. Consequent studies by Bechert et al[4] have shown that the skin friction drag reduction can be as high as 10% through this technique. Recently, Garcia-Mayoral and Jimenez[7–9] introduced a more 'universal' method to characterize riblet drag reduction, based on the groove cross-section area $\ell^+ = (A^+)^{1/2}$. They have shown that an optimum drag reduction is achieved for $\ell^+ \approx 10.7$. In current study however, we use the classical geometric parameters, riblet spacing and riblet height. The drag reduction by riblets is reached through the modification of the near-wall cycle of streaks and streamwise vortices (Kline et al[10] and Robinson[11]) which results in a reduction of the velocity gradient at the wall. Extensive studies by Bechert et al[4] and Luchini et al.[12] have shown that the unique continuous geometry and low-profile of riblets hamper the cross-flow fluctuations of the near-wall cycles and relocate the near-wall streamwise vortices further from the surface resulting in reduced skin friction drag. Apart from influencing the near-wall cycle of streaks and streamwise vortices, recent investigations have also shown that riblets are able to affect Tollmien-Schlichting (TS) waves in laminar flow and constrain the growth of turbulent spots which ultimately lead to the delay in transition from laminar to turbulent flow (Strand and Goldstein[13]). Delaying transition from laminar to turbulence will result in lower skin-friction drag (Joslin[14]).

Recently, a new and unique class of surface modifications with converging and diverging (herringbone) arrangements of riblets inside the surface of a pipe flow was presented by Koeltzsch et al.[15] The herringbone pattern is formed by yawing the riblets in one half of the pipe by $+45^\circ$ to the axial direction, and the other half at -45°. This unconventional pattern was found in nature on the skin surrounding the sensory receptors of sharks, tails of fish, and feathers of birds. Results from this study show that the herringbone riblet pattern causes a large-scale azimuthal variation in the mean velocity and turbulence intensity inside the fully developed turbulent pipe flow. Their work was extended to zero pressure gradient boundary layers by Nugroho et al[16] and it was found that the strength of the spanwise variation is dependent on several parameters, including the viscous-scaled height of the surface perturbation h^+, surface yaw angle α and streamwise fetch F_x (streamwise length of rough surface over which the boundary layer has developed). Koeltzsch et al[15] and Nugroho et al[16] hypothesized that the herringbone directional surfaces generate large-

scale counter-rotating roll-modes / vortices within the turbulent boundary layers. However, the lack of cross-wire / PIV data prevents them from proving this hypothesis. The possibility of a low profile vortex generator could be attractive in situations where it is desirable to introduce vortices into boundary layers (such as for separation control) with a minimum parasitic drag penalty. A recent study by Chen et al[17] shows that the herringbone surface pattern in a fully developed turbulent pipe flow is able to reduce drag by up to 16%, which is significantly higher than standard riblets (10%). In addition Schoppa and Hussain[18] have shown that large-scale counter rotating streamwise vortices are able to significantly reduce skin friction drag by up to 20%, in DNS of turbulent channel flow.

Another application of the herringbone surface pattern is to act as a low-profile device to delay transition from laminar to turbulent flow. The transition from laminar to turbulent flow is caused by the instability of Tollmien-Schlichting (TS) waves. As the TS waves exceed the critical amplitude of 1% of the freestream velocity U_∞, a secondary instability occurs leading to fast transition to turbulence (Herbert[19]). Recent numerical findings by Cosu and Brand[20] show that by introducing certain amplitude streaks, TS waves can be stabilized, hence delaying transition. This has been verified experimentally by generating streaks trough an array of roughness elements in the shape of a cylinder (see Fransson et al[21–23]). The same authors recently extend their work by generating a stronger streaks using miniature vortex generators (MVG) (Fransson and Talamelli[24]). These results suggest a possibility of using the herringbone surface roughness pattern as a mechanism to generate the streaks to delay flow transition.

The aim of the current study is to confirm the large-scale counter rotating roll-modes induced by the herringbone surface roughness pattern in zero pressure gradient turbulent boundary layers. Furthermore, this study is also interested in looking at the behavior of the counter rotating roll-modes when the surface reverts from rough to smooth.

II. Experimental Apparatus

A. Wind Tunnel Facility

The experiments are performed in an open-return blower wind-tunnel located in the Walter Basset Aerodynamics Laboratory at The University of Melbourne. The wind-tunnel has a cross sectional area of 0.94×0.375 m with a 6.7 m long test section. In this study we use the first 5 m of the wind tunnel's test section. The freestream turbulence level is $\approx 0.3\%$, and the ceiling of the working section is adjusted to maintain a zero pressure gradient along the test section. The floor of the tunnel can be lowered using hydraulic lift located under the tunnel to ease the interchange between various rough wall and smooth wall cases.

B. Surface Roughness

Figure 1 shows a schematic diagram of the surface used in this study. The surface consists of alternating strips of yawed riblets at $\pm\alpha$ to form a distinctive herringbone pattern. The riblet spacing and height are $s = 0.675$ mm and $h = 0.5$ mm respectively, giving an h/s ratio of 0.74. Due to limitations in our tools, the trough of the riblets is slightly flat with a length of 0.1 mm. Thus it does not represent the classic triangular profile. It is also noted that the geometry of the riblets in the current study does not have the optimal value for h/s & tip angle β as shown in Bechert et al.[4] The aim of this study is to investigate the ability of these surfaces to generate large-scale secondary flows, we have not attempted to optimize the surface for drag reduction. For the results presented here, the yaw angle that forms the converging and diverging alignment is set at $\alpha = 20°$, which is smaller than the 45° case analyzed in Koeltzsch et al.[15] The choice of using a smaller angle is based on the investigations by Walsh and Lindemann[25] and Hage et al,[26] who have shown that the riblets with yaw angle greater than $25° - 30°$ can cause increases in skin friction. A series of tiles were manufactured to cover the entire test section of the wind-tunnel. A master tile is machined from acetal copolymer using a three-axis CNC machine with a 60° tool bit. The master tile has an overall dimension of 515×295 mm. For the case tested, the width of each converging and diverging region is 73.75 mm, yielding a total spanwise wavelength $\Lambda = 147.5$ mm. A mould of the master tile was made from platinum cured silicone rubber and used to cast multiple polyurethane copies. To ensure favorable mechanical properties, the polyurethane is mixed with aluminum powder. A total of 30 riblet tiles are produced and used to form a test surface that spans the full width of the working section (six complete wavelength) and a distance of

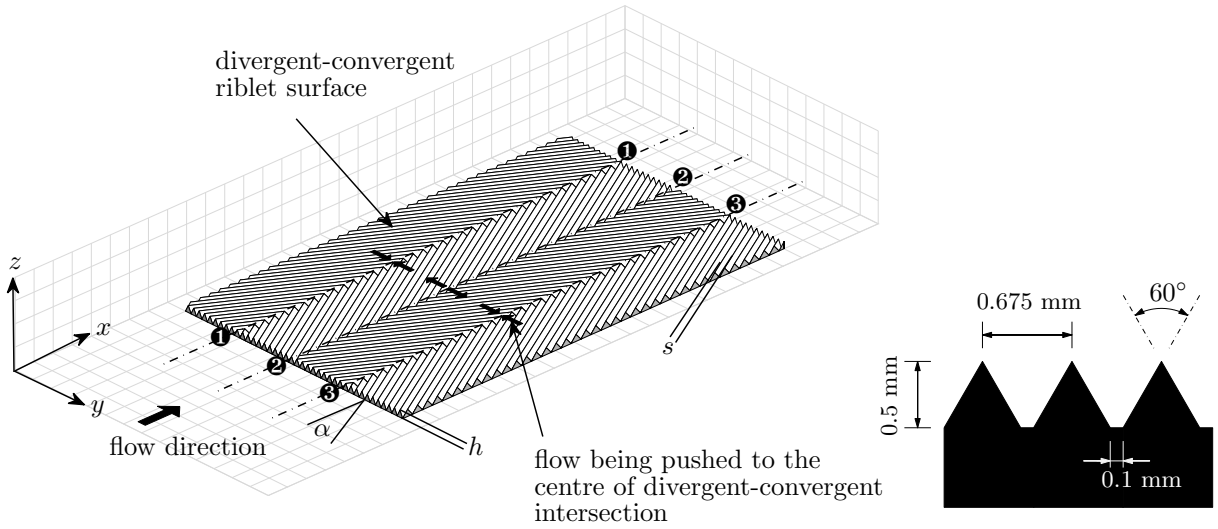

Figure 1. Schematic diagram of the diverging-converging riblet pattern, showing expected regions of converging (regions 1 and 3) and diverging (region 2) spanwise flow. Insert shows the riblet cross section.

5 m downstream of the entry to the working section.

C. Experimental Set-up

Throughout this report, the boundary layer thicknesses δ is calculated based on the wall-normal location where the velocity recovers 98% of the freestream velocity U_∞ (i.e $U/U_\infty = 0.98$). The wall skin friction velocity, $U_\tau = \sqrt{\tau_w/\rho}$, (where τ_w is the wall shear stress and ρ is fluid density). The estimation of U_τ, is discussed in more detail in section IIIA. The subscript + refers to viscous scaling of velocities or heights, such as $U^+ = U/U_\tau$ and $z^+ = zU_\tau/\nu$, where z is wall-normal distance and ν is kinematic viscosity. s^+ is the viscous-scaled riblets spacing, where $s^+ = sU_\tau/\nu$, similarly h^+ is viscous-scaled riblet height, where $h^+ = hU_\tau/\nu$. The subscript s (i.e. δ_s or U_{τ_s}) refers to the smooth-wall case, and the subscript sa (i.e. δ_{sa} or $U_{\tau_{sa}}$) denotes the spanwise averaged value over one complete wavelength Λ of the rough wall surface. The subscript r_s (i.e. δ_{r_s} or $U_{\tau_{r_s}}$) refers to the spanwise averaged value for the rough to smooth wall transition case.

Table 1 lists the riblet parameters and experiment properties of the current study. Here one type of yaw angle α is investigated at two different x locations, $x = 3$ m and $x = 4$ m (Experiments A1 - A2). In this study we are also interested to know whether the large-scale roll-modes persist over the smooth wall downstream of the riblet geometry. In this set of experiments, the rough wall covers the first 3 m of the test section, and the remaining 2 m is covered with smooth wall. The measurements are made at $x = 4$ m and $x = 5$ m (Experiments B1 - B2), where the following smooth-wall distances are $r_s = 1$ m and $r_s = 2$ m respectively. The corresponding fully smooth-wall case at $x = 3$ m, $x = 4$ m and $x = 5$ m is also presented in table 1 (case S1 - S3). The experiment locations are shown in figure 2.

D. Velocity Measurements

The measurements are performed using single-normal hot-wires and cross-wires mounted to an automated two dimensional traverse capable of moving in both the spanwise and wall-normal directions. The hot-wire probes are operated using an in-house Melbourne University constant temperature anemometer (MUCTA). Details of the anemometer design are given in Perry[27] and Perry and Morrison.[28] The single-normal hot-wire probe used is a boundary layer type probe-body geometry 55P15 from Dantec, while the cross-wire probe is 55P61 from the same manufacturer. Both probe sensors consist of 5 µm diameter platinum filament sensors, formed from Wollaston wire with an etched length $l = 1$ mm. The length-to-diameter ratio l/d of the etched hot-wire sensors are equal to (or exceed) 200 to minimize attenuation from end conduction (Ligrani and Bradshaw[29]). The viscous-scaled wire length l^+ is $\approx 36 - 42$, where $l^+ = lU_\tau/\nu$. These values will result in some attenuation due to insufficient spatial resolution (Ligrani and Bradshaw[29] and Hutchins et al[30]).

Exp code	U_∞ (m/s)	x (m)	α (°)	r_s	h^+_{sa}	s^+_{sa}	δ_{sa} (m)	$U_{\tau_{sa}}$ (m/s)	$Re_{\tau_{sa}}$
A1	15.02	3	20	-	21	28	0.0577	0.608	2261
A2	15.17	4	20	-	21	28	0.0737	0.594	2975
							δ_{r_s} (m)	$U_{\tau_{r_s}}$ (m/s)	$Re_{\tau_{r_s}}$
B1	15.02	4	20	1	-	-	0.0714	0.629	3029
B2	15.05	5	20	2	-	-	0.0840	0.598	3310
							δ_s (m)	U_{τ_s} (m/s)	Re_{τ_s}
S1	14.94	3	-	-	-	-	0.0434	0.563	1582
S2	14.90	4	-	-	-	-	0.0499	0.554	1787
S3	14.89	5	-	-	-	-	0.0629	0.545	2255

Table 1. Experimental parameters for rough surface. The Karman number $Re_{\tau_{sa}} = U_{\tau_{sa}}\delta_{sa}/\nu$, viscous-scaled height h^+ and viscous-scaled spacing s^+ are calculated from the spanwise-averaged skin friction velocity $U_{\tau_{sa}}$

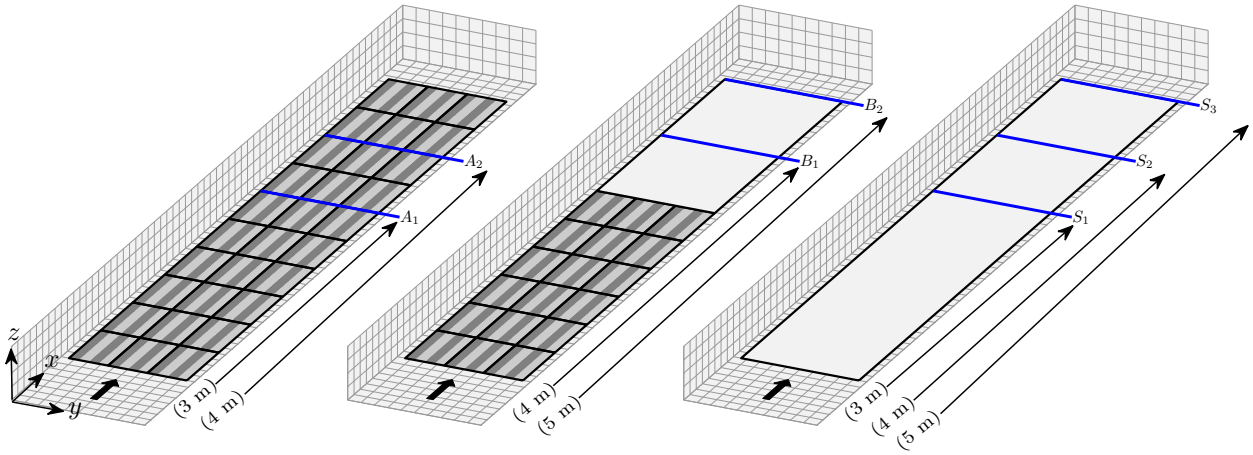

Figure 2. Measurement locations.

However, in this study, which is essentially a comparison of the riblet modified flow to the smooth wall, such attenuation is deemed acceptable.

Two types of measurements are conducted in every case. The first is a wall-normal direction measurement, where 50 logarithmically-spaced points ($0 < z \lesssim 2.5\delta$) are sampled at 50 kHz for 150 seconds, resulting in boundary layer turn-over time of $43000\delta/U_\infty$. The second is a two-dimensional measurement where the sensors are moved in both the wall-normal and spanwise direction. The sensor moves 40 points logarithmically in the wall-normal direction, between $0 < z \lesssim 2.5\delta$, and 21 points in the spanwise direction covering $-\Lambda/2 < y < \Lambda/2$. To minimize hot wire drift and excessive changes in atmospheric conditions, the two dimensional measurements are sampled for relatively short time, 30 seconds at 50 kHz which corresponds to a boundary layer turn-over time of $9000\delta/U_\infty$.

III. Results

A. Experiment A2: General effect of herringbone pattern surface roughness

Figure 3 (a & b) show the variation of the mean velocity and turbulence intensity covering the whole spanwise wavelength Λ of the rough surface for experiment A2. The wall-normal distance is normalized

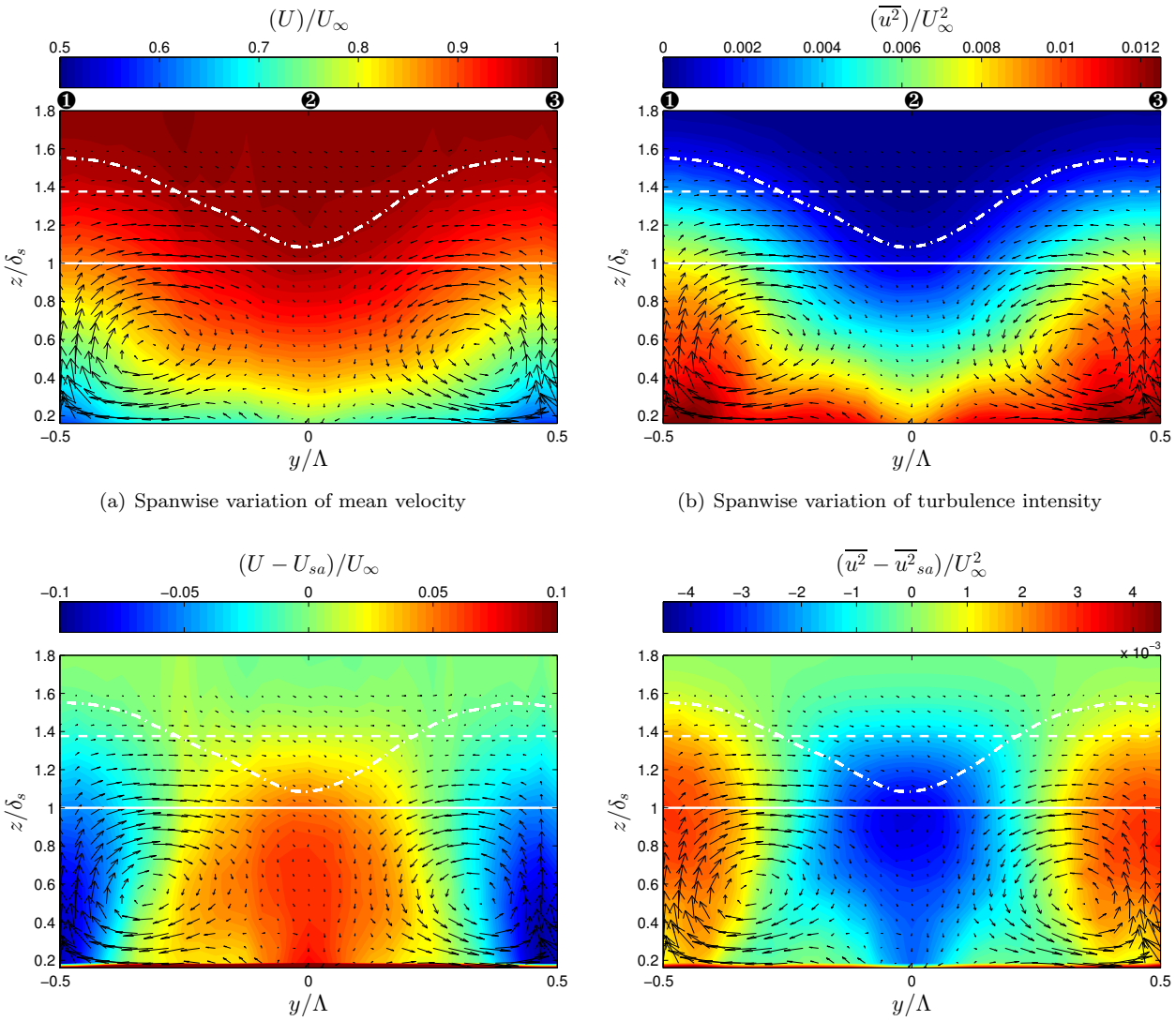

(a) Spanwise variation of mean velocity

(b) Spanwise variation of turbulence intensity

(c) Spanwise averaged of mean velocity

(d) Spanwise averaged of turbulence intensity

Figure 3. Spanwise variation of mean streamwise velocities (a & c) and the turbulence intensities (b & d) for case A2. wall-normal ordinates are non dimensionalised with boundary layer thickness of the corresponding smooth wall δ_s, shown here with solid horizontal line. The boundary layer thickness over rough wall δ_r is represented by the dot-dashed line. The spanwise average thickness of the boundary layer over one spanwise wavelength δ_{sa} is shown with dashed line. The velocity vectors represent the spanwise mean velocity V and the wall-normal mean velocity W.

by the boundary layer thickness of the corresponding smooth wall δ_s. The smooth-wall measurements are performed at the same streamwise location x and freestream velocity U_∞. The circled numbers point out the converging (❶ & ❸) and diverging regions (❷). The counter-rotating vortex pair are visualized via the overlaid vectors of spanwise V and wall-normal W mean velocity components. Both are non-dimensionalized by the freestream velocity U_∞. From figure 3 (a & b) it is clear that the roughness pattern causes a significant spanwise variation in the streamwise mean velocity and turbulence intensity. The boundary layer thickness also varies dramatically along the spanwise wavelength, varying from $\sim 1\delta_s$ at the diverging region to $\sim 1.6\delta_s$ at the converging region. The results confirm the hypothesis that the herringbone surface roughness pattern generates large-scale counter rotating roll-modes.

To further illustrate the effect of the counter rotating roll-modes, figure 3 (c & d) show the spanwise variation in the streamwise mean velocity and the turbulence intensity about their respective spanwise-averaged value at each wall-normal location. The strength of the counter-rotating roll-modes in this particular

case is relatively small, with the maximum values for V and W being around 2% of the freestream velocity. Nevertheless, this relatively weak three-dimensionality is able to disturb and modify the flow everywhere up to the edge of boundary layer. Compared to most other surface roughness configurations, it is surprising (and atypical) that such a small perturbation ($h = 0.01\delta$) can cause such a pronounced modification to the entire turbulent boundary layer. Parametric studies by Nugroho et al[16] show that the strength of the large-scale spanwise variations in the streamwise velocity depend on the viscous-scaled height of the surface perturbation h^+, surface yaw angle α and streamwise fetch F_x. It is believed that the same parameters also affect the strength of the large-scale spanwise variations in the other two velocity components. Further parametric studies for different h^+, α and F_x cases using cross wire or Particle Image Velocimetry (PIV) are required to support this hypothesis. The effect of the spanwise wavelength Λ is also under investigation.

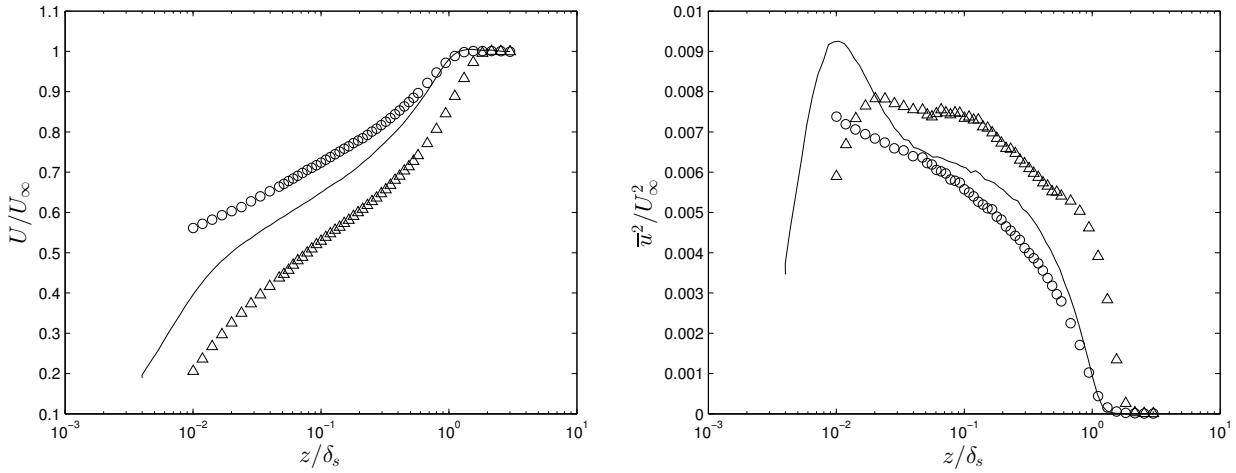

(a) Mean velocity profile

(b) turbulence intensity profile

Figure 4. Mean velocity and turbulence intensity profiles for cases A2 and S2. Both mean velocity and turbulence intensity are normalized using the freestream velocity, and wall-normal distance is normalized by the boundary layer thickness of the corresponding smooth wall. Symbols represent the rough surface data ($\circ$) **for the diverging region and** (Δ) **for the converging region. Solid line shows the smooth wall case at similar freestream velocity U_∞ and streamwise location x**

From figure 3 it is clear that over the converging region the flow is being forced to converge together and move away from the wall (forming common-flow-up). This common-flow-up carries relatively high near-wall turbulent fluctuations to the outer region of the boundary layer and causes higher local turbulence intensity over this region. The upward flow also carries the slow moving fluid further from the wall, resulting in low local mean velocity and a thicker boundary layer. Over the diverging region, the flow is being forced to diverge outwards, causes higher speed fluid (which has low turbulence intensity) to move towards the wall (forming common-flow-down) and confining the turbulent fluctuations closer to the wall. This mechanism reduces the local turbulence intensity above this region. The common-flow-down also forces the fast moving fluid to move closer to the wall causing a higher local mean velocity and thinner boundary layer. We note that these results are consistent with Koeltzsch et al[15] and Nugroho et al[16] findings.

Figure 4a compares the mean streamwise velocity profiles over the diverging and converging regions for case A2 and the corresponding smooth wall (S2). The wall-normal distance is normalized with the smooth-wall boundary layer thickness δ_s, and the mean velocity is non-dimensionalized with freestream velocity U_∞. From this figure it is obvious that the surface roughness has caused a significant modification in the mean velocity. The local mean velocity above the diverging region is higher everywhere than the smooth-wall case, while over the converging region the local mean velocity is lower everywhere across the boundary layer. Figure 4b shows the turbulence intensity modification for the same case. The turbulence intensitites are normalized with the square of the freestream velocity. This figure clearly shows that over the diverging region, the turbulence intensity is lower everywhere compared to the smooth wall case. This behavior is consistent with the current hypothesis that the common-flow-down carries the relatively low turbulent fluctuations from the outer region towards the wall, and confines the turbulent fluctuations closer to the surface. Over the converging region, for the majority of the layer, the turbulence intensity is higher than the

corresponding smooth wall. This condition occurs because the common-flow-up carries the highly turbulent near-wall fluctuations away from the wall, resulting in increased fluctuations across the layer.

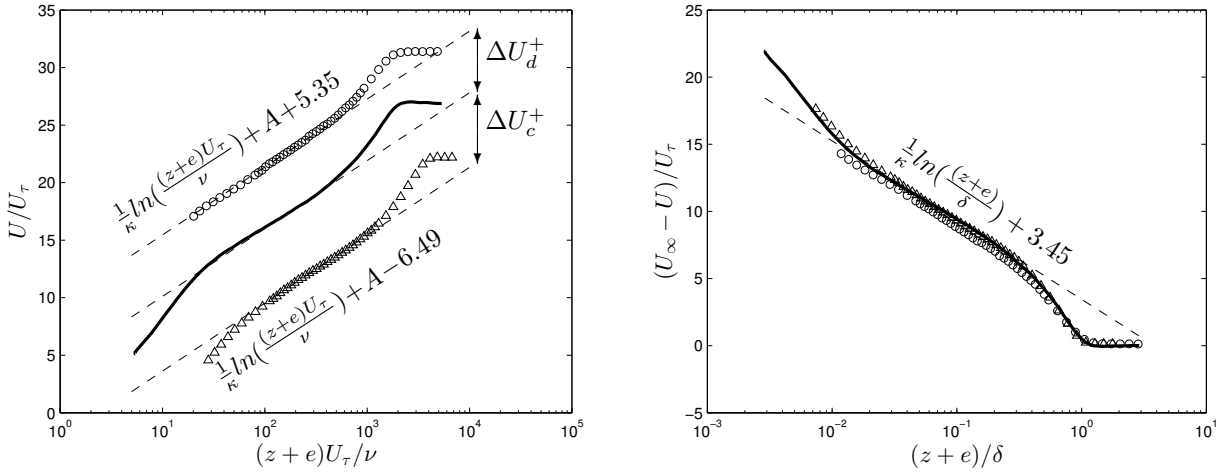

(a) Mean velocity profile

(b) Velocity defect profile

Figure 5. Mean velocity and velocity defect profiles for case A2 and S2. Symbols represent the rough surface data ($\circ$) for the diverging region and (Δ) for the converging region. Solid lines show the smooth wall case at similar condition.

In turbulent boundary layers, it is desirable to have a velocity and length scale based on the wall shear-stress (i.e U_τ and ν/U_τ). For the smooth wall case the skin friction velocity can be obtained using the Clauser method, where the mean velocity profile is fitted to the logarithmic law with constant $\kappa = 0.39$ and intercept $A = 4.2$ (from Perry and Li[31]). Determining skin friction velocity over a rough wall condition is much more problematic. To obtain the skin friction value over the rough case (U_τ) we use the modified Clauser technique, where the logarithmic region of the mean profile is fitted to the following modified rough-wall relationship,

$$\frac{U}{U_\tau} = \frac{1}{\kappa}\log\frac{(z+e)U_\tau}{\nu} + A - \frac{\Delta U}{U_\tau}. \tag{1}$$

Here, e is the roughness offset and $\Delta U/U_\tau$ is the roughness function. The difficulty in using this method is there are three free parameters, U_τ, e, and ΔU. In some previous studies a constant value of e has been assumed based on the shape of the riblet cut, i.e $0.25h$ for triangular and $0.37h$ for scalloped riblets (see Bechert et al[32] and Choi[2]). Based on these results, we use a constant value of $0.25h$ throughout this analysis as the riblet cross section closely resembles the triangular shape. Aside from the uncertainty in fitting data to equation 1, there are also more fundamental questions surrounding whether or not it is correct to assume a logarithmic behavior in the mean velocity profiles, for flows with a strong spanwise periodicity. Indeed our results have shown that for some of the stronger perturbation cases (such as high angle α and h^+), the logarithmic behavior in the mean velocity profile is ill defined, making the application of modified Clauser technique questionable. Conservatively, we estimate that the error in determining U_τ through this modified Clauser technique can be as high as 10%. However, for this study and in the absence of more reliable direct methods, such estimates provide a useful indication of the likely variation in skin friction velocity. For all of the rough wall (A1 & A2) and rough-to-smooth wall (B1 & B2) cases listed in table 1, the friction velocity is spanwise averaged over one wavelength Λ of the herringbone pattern (covering the converging-diverging-converging region).

Figure 5a shows the viscous-scaled modified velocity profiles for case A2 and S2, and figure 5b shows the velocity defect profiles. Figure 5a clearly shows the difference in the friction velocity and roughness behavior of the converging and diverging region. A pronounced downward shift over the converging region (positive $\Delta U/U_\tau$) indicates an increase in wall drag for this region of the surface. Over the diverging region however, the upward shift (negative $\Delta U/U_\tau$, or negative roughness) suggests a decrease in wall drag. It is surprising that such a high negative roughness function can be achieved. Negative roughness functions are observed

over conventional riblet surfaces (Choi[2]), but in these cases the shift was very small ($\Delta U/U_\tau \approx -1$). Figure 5b shows that the velocity defect profiles over the converging and diverging region do not collapse to the corresponding smooth wall. This indicates shows that Townsend's outer layer similarity hypothesis does not hold for this type of roughness. This is not surprising in this case since the roughness has imposed high degree of three-dimensionality that extends all the way across the layer, contravening the first assumption of Townsend's original similarity hypothesis for rough walls.

B. Experiment A1, B1 and B2 : Rough to smooth wall case

In the previous section we have demonstrated the capability of the herringbone surface roughness pattern to generate large-scale counter rotating vortices. This ability could be attractive for practising engineers to apply in various engineering applications, such as to replace traditional vortex generators on an aircraft wing. However, it will be more economical if we can maintain these roll-modes without covering the whole surface of interest, for example, applying the surface roughness to the appropriate region of the upper surface of an airfoil to influence separation. Furthermore, considering the slight net increase of the wall drag on the surface itself, it will be more beneficial to use this roughness only at critical locations. Motivated by such considerations, we are interested to observe the behavior of the large-scale roll-modes when the surface reverts to the smooth case. In particular, we attempt to understand whether these large-scale roll-modes persist on the smooth wall downstream of the roughness pattern.

For this experiment, the roughness pattern covers the first 3 m of the test section after which the surface reverts to smooth wall (see figure 2). Three sets of measurements are performed, at $x = 3$ m (case A1, located above the roughness), at $x = 4$ (case B1, located above smooth wall, with rough-to-smooth distance $r_s = 1$ m or $\sim 20\delta_s$), and at $x = 5$ (case B2, located above smooth wall, with rough-to-smooth distance $r_s = 2$ m or $\sim 40\delta_s$). The 3 m roughness development has been shown in the previous study to generate a relatively strong spanwise variation (see Nugroho et al[16]). Figure 6 (a - f) show the results from experiments A1, B1 and B2 respectively. The left-hand column shows the contour plots of the mean velocity variation about the spanwise averaged values and the right-hand side column shows the contour plots of the turbulence intensity variation about the spanwise averaged values. The overlaid vectors represent the spanwise V and wall-normal W mean velocity components normalized with the freestream velocity U_∞. In this set of experiments, since we are moving the measurements point further downstream, the friction Reynolds number Re_τ will vary significantly (refer to table 1). Figure 6 reveals that as the flow moves from the rough surface to the smooth surface, the strength/magnitude of the perturbation diminishes. Interestingly however, the large-scale roll-modes still persist even at $40\delta_s$ (case B2) and are able to cause a relatively large spanwise variation in the boundary layer thickness ($\approx 45\%$ variation between converging and diverging surface). Furthermore, the overall size of the region of the spanwise variation and hence the roll-modes seems to remain relatively constant.

IV. Summary and conclusion

A study of zero pressure gradient turbulent boundary layers over a herringbone pattern riblet-type surface roughness has been performed. The results confirm the hypothesis that this class of surface roughness generates large-scale roll-modes within the turbulent boundary layer resulting in a dramatic spanwise modification to the streamwise mean velocity, turbulence intensity and the boundary layer thickness. The results reveal that over the converging region, the flow is forced to converge together and move away from the wall, creating a common-flow-up portion of the counter-rotating vortex (despite the small roughness height 0.01δ). The common flow up carries the relatively slower and highly turbulent fluid further from the wall, resulting in lower streamwise mean velocity and high turbulence intensity over this region. Above the diverging section the flow moves towards the wall from the outer region (where the fluid flow is faster and has low turbulent fluctuations), forming the common-flow-down part of the roll modes. The high and low velocity region causes a pronounced spanwise variation in boundary layer thickness. Over the diverging region the boundary layer thickness is thinner than over the converging region. Although the strength of the spanwise V and wall-normal W velocity components of the counter rotating vortex are relatively small ($\approx 2\%$ of U_∞), they are able to cause a significant large-scale modification to the turbulent boundary layer.

From previous parametric studies by Nugroho et al,[16] it is found that the strength of the spanwise periodicity increases with the surface yaw angle α, viscous-scaled riblet height h^+ and streamwise fetch F_x.

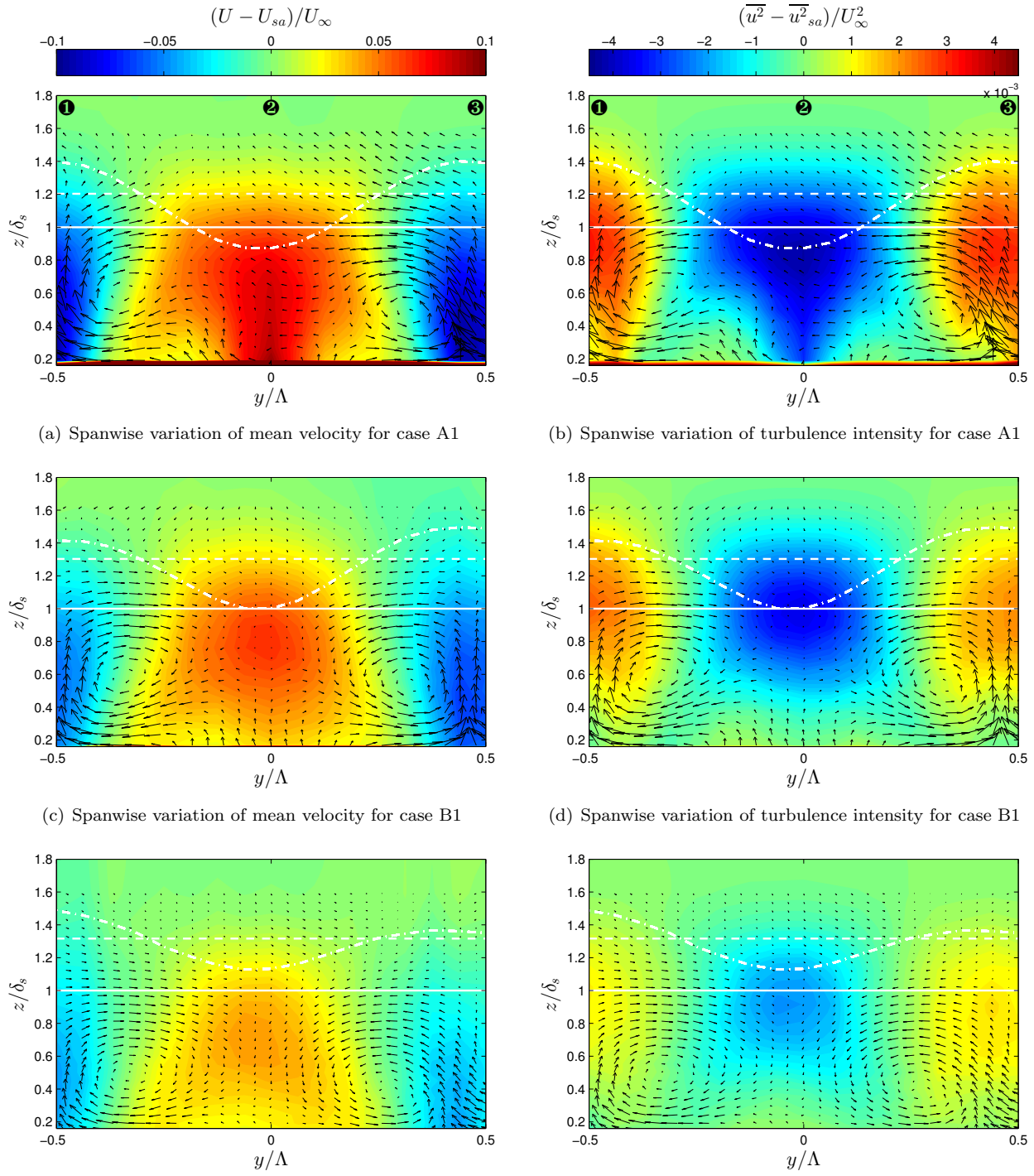

(a) Spanwise variation of mean velocity for case A1

(b) Spanwise variation of turbulence intensity for case A1

(c) Spanwise variation of mean velocity for case B1

(d) Spanwise variation of turbulence intensity for case B1

(e) Spanwise variation of mean velocity in for case B2

(f) Spanwise variation of turbulence intensity for case B2

Figure 6. Spanwise variation of mean velocities (left-hand-side) and the turbulent intensities (right-hand-side) for case A1, B1 and B2. wall-normal ordinates are non dimensionalized using boundary layer thickness of the corresponding smooth wall δ_s, shown here with straight horizontal line. The boundary layer thickness over rough wall δ_r is represented by the dot-dashed line. The spanwise average boundary layer thickness over one spanwise wavelength δ_{sa} is shown with dashed line. The velocity vectors represent the spanwise mean velocity V and the wall-normal mean velocity W. All velocity components are normalized with freestream velocity U_∞

In this report we have investigated another parameter, namely the rough-to-smooth distance r_s when the surface condition reverts from the herringbone pattern to the smooth case. An increase in r_s shows a lower

spanwise variation of mean velocity and turbulence intensity. However, the roll-modes, though weakened, clearly persist beyond $40\delta_s$ downstream of the rough-to-smooth transition.

The herringbone surface pattern offers a novel method of generating counter rotating roll-modes within turbulent boundary layers. Such surfaces may eventually present an interesting addition to the various technique of controlling boundary layer flows. By fine tuning the parameters of the surface, it should be possible to produce roll-modes with strengths tailored to specific applications. Further parametric studies, such varying Λ and riblet geometry (scalloped and blade) investigated using cross-wire, PIV and a drag balance are deemed important in order to better understand this type of directional roughness.

Acknowledgments

This research was supported under the Australian Research Council's Discovery Projects (project number DP110102448) and Future Fellowship funding schemes (project numbers FT110100432 and FT120100409).

References

[1]M J Walsh. Turbulent boundary layer drag reduction using riblets. *AIAA Journal*, 82-0169, 1982.

[2]K S Choi. Near-wall structure of a turbulent boundary layer with riblets. *J. Fluid Mech*, 208:417–458, 1989.

[3]D W Bechert and M Bartenwerfer. The viscous flow on surfaces with longitudinal ribs. *J. Fluid Mech*, 206:105–129, 1989.

[4]D.W. Bechert, M. Bruse, W. Hage, J. G. Van Der Hoeven, and G. Hoppe. Experiments on drag-reducing surfaces and their optimisation with an adjustable geometry. *J. Fluid Mech*, 338:59–87, 1997.

[5]B Dean and B Bhushan. Shark-skin surfaces for fluid-drag reduction in turbulent flow: a review. *Phil. Trans. R.Soc. Lond. A*, 368:4775 – 4806, 2010.

[6]M J Walsh. Riblets as a viscous drag reduction technique. *AIAA Journal*, 21:485 – 486, 1983.

[7]R Garcia-Mayoral and J Jimenez. Drag reduction by riblets. *Phil. Trans. R.Soc. Lond. A*, 369:1412–1427, 2011.

[8]R Garcia-Mayoral and J Jimenez. Hydrodynamic stability and breakdown of the viscous regime over riblets. *J. Fluid Mech*, 678:317 – 347, 2011.

[9]R Garcia-Mayoral and J Jimenez. Scaling of turbulent structures in riblet channels up to $re_\tau \approx 550$. *Phys. Fluids*, 24:105101, 2012.

[10]S J Kline, W C Reynolds, F A Schraub, and P W Rundstadler. The structure of turbulent boundary layers. *J. Fluid Mech*, 30:741–773, 1967.

[11]S K Robinson. Coherent motions in turbulent boundary layers. *Annual Review of Fluid Mechanics*, 23:601–639, 1991.

[12]P Luchini, F Manzo, and A Pozzi. Resistance of a grooved surface to parallel flow and cross-flow. *J. Fluid Mech*, 228:87 – 109, 1991.

[13]J S Strand and D B Goldstein. Direct numerical simulations of riblets to constrain the growth of turbulent spots. *J. Fluid Mech*, 668:267 – 292, 2011.

[14]R D Joslin. Aircraft laminar flow control. *Annual Review of Fluid Mechanics*, 30:1 – 29, 1998.

[15]K Koeltzsch, A Dinkelacker, and R Grundmann. Flow over convergent and divergent wall riblets. *Exp. Fluids*, 33:346–350, 2002.

[16]B Nugroho, N Hutchins, and P Monty, J. Large-scale spanwise periodicity in a turbulent boundary layer induced bu highly ordered and directional surface roughness. *International Journal of Heat and Fluid Flow*, 41:90 – 102, 2013.

[17]H Chen, F Rao, X Shang, D Zhang, and I Hagiwara. Biomimetic drag reduction study on herringbone riblets of bird feather. *Journal of Bionic Engineering*, 10:341 – 349, 2013.

[18]W. Schoppa and F. Hussain. A large-scale control strategy for drag reduction in turbulent boundary layers. *Phys. Fluids*, 10, 5:1049–1051, 1998.

[19]T Herbert. Secondary instability of boundary layers. *Annual Review of Fluid Mechanics*, 20:487 – 526, 1988.

[20]C Cossu and L Brandt. Stabilization of tollmien-schlichting waves by finite amplitude optimal streaks in the blasius boundary layer. *Phys. Fluids*, 14:8:57 – 260, 2002.

[21]J. H. M. Fransson, A. Talamelli, L. Brandt, and C. Cossu. Experimental and theoretical investigation of the nonmodal growth of steady streaks in a flat plate boundary layer. *Phys*, 16:3627, 2004.

[22]J. H. M. Fransson, A. Talamelli, and C. Cossu. Experimental study of the stabilization of tollmien-schlichting waves by finite amplitude streaks. *Phys*, 17:054110, 2005.

[23]J. H. M. Fransson, A. Talamelli, L. Brandt, and C. Cossu. Delaying transition to turbulence by a passive mechanism. *Phys. Rev. Lett.*, 96:064501, 2006.

[24]J. H. M. Fransson and A. Talamelli. On the generation of steady streamwise streaks in flat-plate boundary layers. *J. Fluid Mech*, 698:211–234, 2012.

[25]M J Walsh and A M Lindemann. Optimization and application of riblets for turbulent drag reduction. *AIAA Journal*, 84 - 0347, 1984.

[26]W Hage, D W Bechert, and M Bruse. Yaw angle effects of optimized riblets. *Proceedings of CEAS/DragNet European Drag Reduction Conference, postdam*, 2000.

[27]A E Perry. *Hot-wire Anemometry*. Oxford University Press, Oxford UK,, 1982.

[28]A E Perry and G L Morrison. A study of the constant temperature hot-wire anemometer. *J. Fluid Mech*, 47:577 – 599, 1971.

[29]P M Ligrani and P Bradshaw. Spatial resolution and measurement of turbulence in the viscous sublayer using subminiature hot-wires probes. *Exp. Fluids*, 5:407–417, 1987.

[30]N Hutchins, T B Nickels, I Marusic, and M S Chong. Hot-wire spatial resolution issues in wall-bounded turbulence. *J. Fluid Mech*, 635:103–136, 2009.

[31]A E Perry and J Ds Li. Experimental support for the attached-eddy hypothesis in zero-pressure-gradient turbulent boundary layers. *J. Fluid Mech*, 218:405 – 438, 1990.

[32]D.W. Bechert, G. Hoppe, and W. E Reif. On the drag reduction of the shark skin. *AIAA Journal*, 85-0546, 1985.